NEGATIVE REFLECTION: A PATH TO VIRTUAL SEISMIC ACQUISITION

LUC T. IKELLE

CASP Project, Department of Geology and Geophysics, Texas A&M University, College Station, Texas 77843-3115, U.S.A. ikelle@icasp.tamu.edu

(Received August 22, 2008; accepted March 12, 2009)

ABSTRACT

Ikelle, L.T., 2009. Negative reflection: a path to virtual seismic acquisition. *Journal of Seismic Exploration*, 18: 199-214.

We here describe one way of constructing data with sources and receivers inside the subsurface from standard data with sources and receivers near the sea surface for offshore, or at the earth's surface for onshore. This construct is based on the recently introduced concept of negative reflection. Negative reflection reflections (also known as virtual events) are wave-scattering events whose first and last bends of wave-propagation paths are parallel. Such events are not recorded in seismic wave-scattering experiments, but they can be constructed from seismic data. When the negative reflection data are used together with seismic data, the abnormal bending of negative reflections allows us to simulate situations in which sources and receivers are located in the subsurface. The benefits of putting the sources and receivers in the ground includes improving the imaging of deep reflectors such as below-subsalt reflectors and below-subbasalt reflectors.

KEYWORDS: virtual events, negative reflection, Snell's law, scattering diagrams, convolutive-type representation theorem, correlation-type representation theorem, seismic data acquisition.

INTRODUCTION

Erez (2006), Ikelle (2004, 2006), and Ikelle and Gangi (2005, 2007) have recently discovered new types of scattering events and showed, through the analysis of the scattering diagrams of the correlation-type representation theorem in inhomogeneous media, that these scattering events obey basic physical laws

0963-0651/09/$5.00

such as Snell's law. They also link these new scattering events with the notion of negative refraction in optics (Pendry et al., 1999; Shelby et al., 2001; Smith et al., 2004; and Veselago, 1968) and that of virtual particles in quantum field theory (e.g., Jones, 2002). Just like the Feynman diagrams in quantum field theory, the scattering diagrams used in these analysis are a schematic form of wave propagation that allows us to understand and develop the wave-scattering theory and its applications in simple and natural terms rather than only in an abstract mathematical way.

The new scattering events are called virtual-reflection events because they are not directly recorded in standard seismic data acquisition. These events are alternatively called negative-reflection events because they are analogous to the recently discovered negative refraction index in optics (Pendry et al., 1999; Shelby et al., 2001; Smith et al., 2004; and Veselago, 1968). Note that the concept of negative-reflection events here is much more complex than that of the negative refraction index in optics because we are dealing with multiple reflectors with arbitrary shapes. Moreover, the concept of negative reflection here includes all possible scattering types, including diffractions.

Our objective here is to describe how the negative reflection events can be used to construct "virtual" acquisition experiments with sources and receivers inside the subsurface. The benefits of such virtual acquisition experiments for seismic-data processing include increasing the signal-to-noise ratio of seismic data, and more-accurate wavefield decomposition, velocity estimation, and imaging of deep reflectors like those located below complex salt bodies or below basalt. We will start our description of virtual acquisitions by a review of seismic diagrammatica*, as the understanding of these diagrammatica is essential for the description of our virtual-acquisition experiments.

* Diagrammatica here mean a collection of scattering diagrams used to describe seismic events. We obviously expect this collection to grow significantly in the coming years in such a way that we will be able to describe the entire field of petroleum seismology by using scattering diagrams.

SEISMIC DIAGRAMMATICA WITH NEGATIVE REFLECTIONS

Examples of the wave-propagation paths which constitute towed-streamer data are depicted in Fig. 1. These events can be grouped into three categories: primaries, free-surface-reflection events (ghosts and free-surface multiples), and internal multiples. Primaries are seismic events which reflect or diffract only once in the subsurface, but not at the free surface, before being recorded. Free-surface-reflection events (ghosts and free-surface multiples) are events with at least one reflection at the sea surface in their wave-propagation path. When the first and/or last reflection in the wave-propagation path of a free-surface-reflection event is at the sea surface, the free-surface-reflection event is

characterized as a ghost. All other free-surface-reflection events are characterized as free-surface multiples. Internal multiples are seismic events with no reflection at the free surface but with reflections between two interfaces other than the free surface. Two types of events in seismic data do not readily fall into the three categories that we have defined. Those events are head waves and direct waves. We treat head waves here as internal multiples and direct waves as primaries.

The key processes of marine seismic imaging (which are at the heart of modern oil and gas exploration and production) include (i) removing free-surface-reflection events from the data and leaving primaries and internal multiples, (ii) removing internal multiples from the data and leaving primaries, and then (iii) locating the scattering points and reflectors inside the subsurface, which are the sources of primaries and internal multiples in particular. All these processes can be explained, derived, and optimized using scattering diagrams (diagrammatica) in a way similar to the way the quantum field theory is often explained using Feynman diagrams.

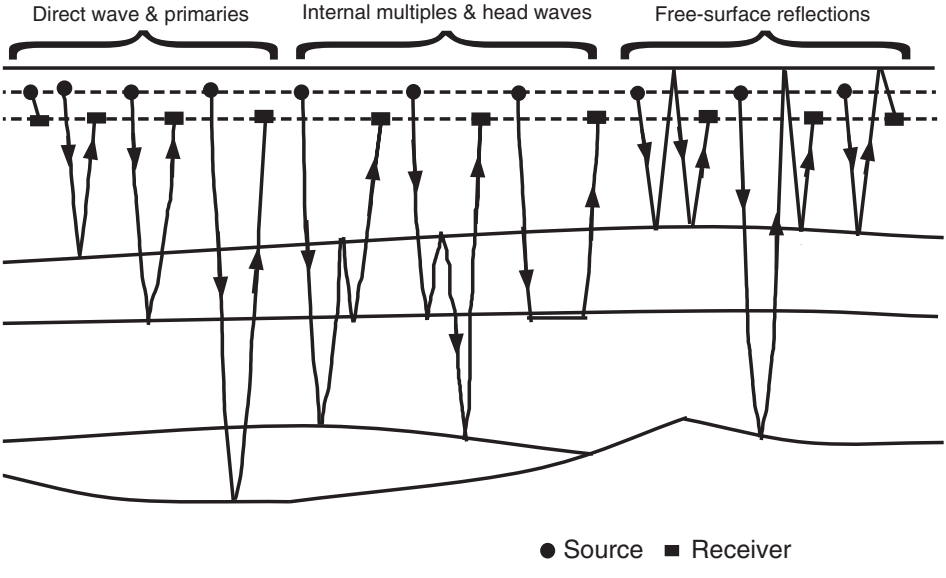

Fig. 1. Examples of the scattering diagrams for direct wave, primaries, free-surface reflections, and internal multiples.

Before we describe the convention used in drawing our scattering diagrams, let us recall that solutions of wave equations (wave equations are the building blocks of seismology) involve waves traveling in positive as well negative time, the so-called "retarded" and "advanced" waves. Retarded waves progressively move with increasing time, as visualized in the classical movies of wave propagation (e.g., Ikelle and Amundsen, 2005). They are consistent with the way current seismic-data acquisitions are carried out; they arrive at receiver locations at some time after they have left the source location. Advanced waves travel backward in time; that is, they arrive at the hydrophones

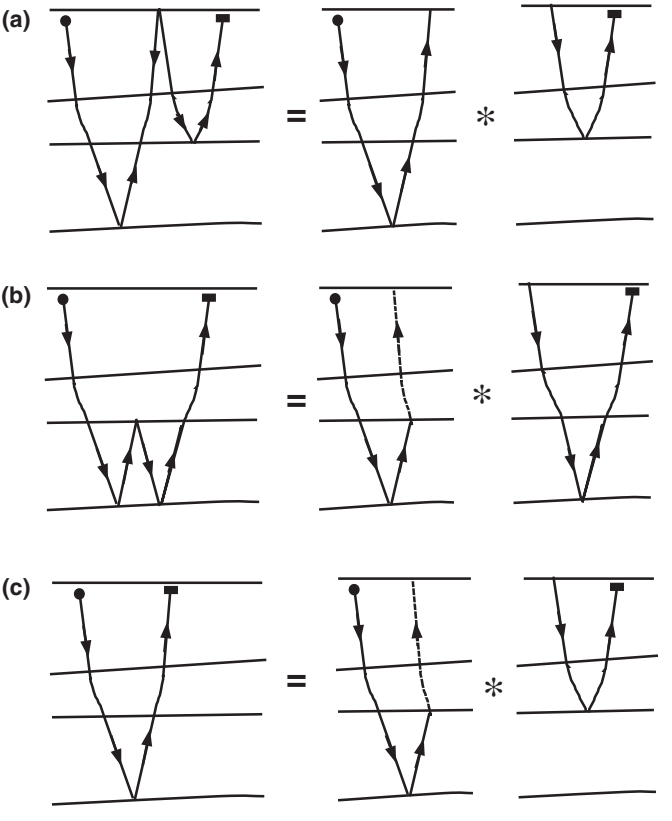

Fig. 2. Examples of constructions of primaries, free-surface multiples, and internal multiples using scattering diagrams. In these scattering diagrams, like the ones in the remaining figures in this paper, the process of wave propagation begins on the left and ends on the right. The solid line represents waves traveling forward in time, and the dotted line represents waves traveling backward in time. (a) A combination of two primaries is used to predict a first-order multiple. Notice that it is always possible to construct free-surface-reflection events by combining the wave-propagation paths of two real events contained in the same seismic data because the wave-propagation paths of free-surface-reflection events contain at least one reflection point at the sea surface. (b) A combination of a primary with a virtual event can produce an internal multiple. (c) This combination can also produce primaries. Notice that the virtual event allows us to compensate for the fact that internal multiples and primaries do not contain free-surface-reflection points.

or geophones before they have left the source point. These waves are really an affront to our common sense and our understanding of how the world operates - our ever-aging bodies being an obvious testimony. So despite the fact that advanced waves are valid solutions to wave equations, they are generally ignored in most seismology studies, at least in part, because of their counterintuitive nature. One of the key features of our diagrammatica here is that these advanced waves are included in our constructions of the scattering diagrams of seismic events.

In our scattering diagrams, such as the ones in Figs. 2 and 3, the process of wave propagation begins on the left and ends on the right. The solid line represents waves traveling forward in time (forward wave propagation), and the dotted line represents waves traveling backward in time (backward wave propagation). In forward wave propagation, the process begins on the left and ends on the right, whereas in backward wave propagation, it is the opposite. The arrows are added in these scattering diagrams to clearly indicate the direction of wave propagation. The point at which two lines meet is known as the scattering point. Scattering points can occur at the intersection of two solid lines, of two dotted lines, or of a solid line and a dotted line. The time is not explicitly shown in the scattering diagrams of this paper in order to avoid an unnecessary complication associated with a third axis. Notice that all events recorded in seismic data (i.e., direct waves, primaries, ghosts, and multiples) have a forward propagation. Therefore, in our diagrammatica, these events will be entirely marked by solid lines and will go from left to right. We will call them "real events" or "positive-reflection events". Their noncausal versions, which correspond to backward propagation, will be marked by dotted lines and will go from right to left. We will call them "anticausal events". Events which combine solid and dotted lines in their constructs will appear only in intermediate, unobservable stages of a process for constructing a real event. We will call these events "virtual events" or "negative-reflection events". Virtual events are central to our construction of virtual acquisitions here.

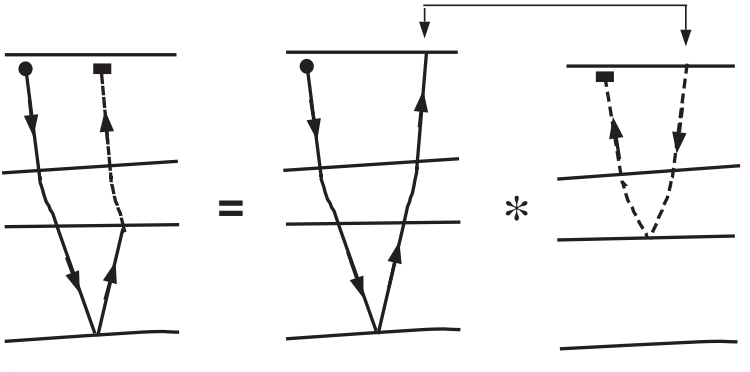

Fig. 3. An illustration of the construction of virtual seismic data as a combination of two primaries in which one of the primaries has been time-inverted.

Mathematical construct of real events

Suppose that we have recorded pressure along with the vertical component of the particle velocity (see the Appendix for the case in which only the pressure wavefield is recorded). Let $P(\mathbf{x},\omega;\mathbf{x}_r)$ and $v_3(\mathbf{x},\omega;\mathbf{x}_s)$ denote the recorded pressure wavefield and the recorded vertical component of the particle velocity, respectively, in the frequency-space (F-X) domain at the source point $\mathbf{x}_s$ and receiver point $\mathbf{x}_r$. We can predict real events with reflections at the free surface as follows:

$$P_M(\mathbf{x}_r,\omega;\mathbf{x}_s) = a(\omega) \int_{S_0} dS(\mathbf{x}) P(\mathbf{x},\omega;\mathbf{x}_r) v_3(\mathbf{x},\omega;\mathbf{x}_s) \quad , \tag{1}$$

where $a(\omega) = 1/s(\omega)$ is the inverse source signature and S_0 is the air-water surface. The pressure field of free-surface reflection events P_M is obtained as the multidimensional convolution of P and v_3. One can also predict free-surface-reflection events of the particle velocity by replacing $P(\mathbf{x},\omega;\mathbf{x}_r)$ in (1) with the corresponding component of the particle velocity, say, $v_i(\mathbf{x},\omega;\mathbf{x}_r)$. Fig. 4 illustrates, with scattering diagrams, how (1) predicts free-surface-reflection events. Basically, the multidimensional convolution of the three events of v_3 (α_i) with the two events of P through eq. (1) allows us to predict free-surface events γ_{ij} ($\gamma_{ij} = \alpha_i * \beta_j$). This multidimensional convolution is entirely based on real events, and it produces only real events.

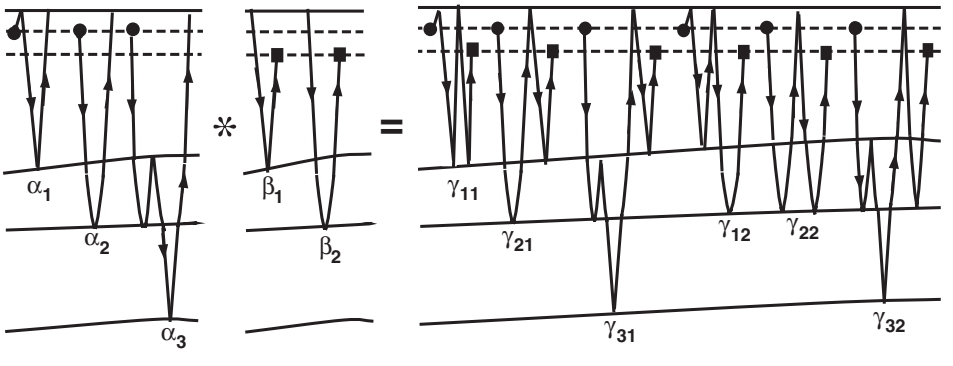

Fig. 4. Examples of the construction of free-surface reflections as a combination of events of the pressure data which contain only primaries (β_i) and the events of the vertical component of particle velocity (α_j). The symbol * denotes the multidimensional convolution operation in (1) operation in the second term of eq. (??), which allows us to combine P_P and v_3. The results of the multidimensional convolutions of P_P and v_3 are denoted γ_{ij} such that $\gamma_{ij} = \alpha_i * \beta_j$. The same nomenclature is used in Figs. 5 and 6.

Mathematical construct of virtual events

The pressure field of virtual events is generally defined as follows:

$$P_V(\mathbf{x}_r,\omega;\mathbf{x}_s) = \int_{S_0} dS(\mathbf{x})P^{-1}(\mathbf{x},\omega;\mathbf{x}_r)v_3(\mathbf{x},\omega;\mathbf{x}_s) \quad , \tag{2}$$

where P_V denotes the virtual data. The field P^{-1} can be estimated as follows:

$$\int_{S_0} dS(\mathbf{x})A(\mathbf{x}_s,\omega,\mathbf{x})P^{-1}(\mathbf{x},\omega,\mathbf{x}_r) = P(\mathbf{x}_s,\omega,\mathbf{x}_r) \quad , \tag{3}$$

where

$$A(\mathbf{x}_s,\omega,\mathbf{x}) = \int_{S_0} dS(\mathbf{x}')P^*(\mathbf{x}_s,\omega,\mathbf{x}')P(\mathbf{x}',\omega,\mathbf{x}) \quad . \tag{4}$$

The asterisk * denotes a complex conjugate. Basically P^{-1} is the normalized complex conjugate of P. Thus a computation of virtual events is a multidimensional normalized crosscorrelation of P with v_3. We can also construct the particle-velocity field of virtual events by replacing $P(\mathbf{x},\omega;\mathbf{x}_r)$ in (2)-(4) by the corresponding component of the particle velocity, say, $v_i(\mathbf{x},\omega;\mathbf{x}_r)$.

Let us now examine the scattering events created during the computation of the scattering integral over S_0 for eq. (2). Fig. 5a shows that the crosscorrelation of the primaries contained in P (i.e., β_1 and β_2) with v_3 (i.e., α_1, α_2, and α_3) allows us to predict virtual events (i.e., $\tilde{\gamma}_{21}$, $\tilde{\gamma}_{31}$, and $\tilde{\gamma}_{32}$), and anticausal virtual events (i.e., $\tilde{\gamma}_{12}$) are also created during the integration over S_0. Fig. 5b shows that we can obtain new configurations of virtual events, sometimes strange-looking virtual events, by simply including free-surface-reflection events in the particle-velocity field. Even more complex configurations can be obtained by including free-surface-reflection events in the pressure field. Nevertheless, these virtual events follow the same patterns as those in Fig. 5a. Basically, the first part of the wave-propagation path of these events follows the normal forward propagation, and the second part follows a backward propagation path, or vice versa.

Note that in all the scattering diagrams of virtual events that we have presented so far, the negative bend is located on the receiver side. We will call such events receiver-side virtual events. By interchanging source and receiver locations in (2)-(4) and in Figs. 3 and 5, the negative bend (dotted line) of virtual events will move to the source side. We will call such events source-side virtual events. Fig. 6 shows receiver-side and source-side virtual events. The multidimensional convolution of these two events produces another strange-

looking event. In terms of virtual acquisition, it simulates two simultaneous virtual experiments if the sources and receivers are at the same depth, as we describe later.

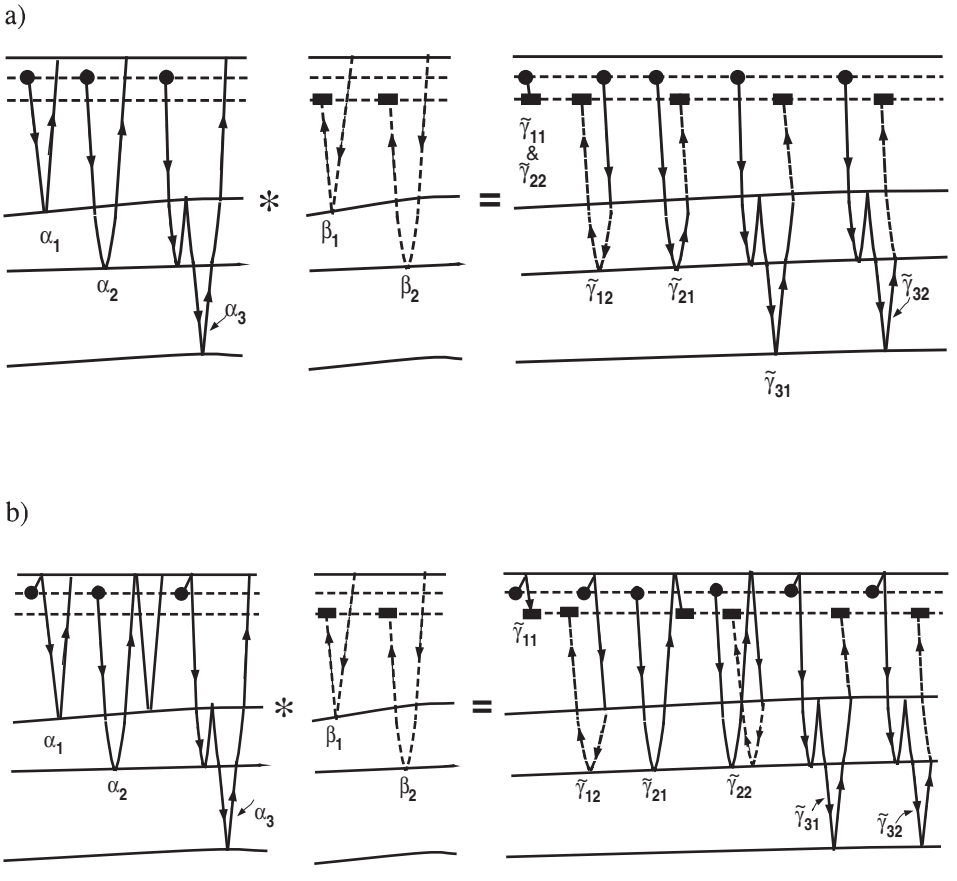

Fig. 5. (a) Examples of the construction of virtual-reflection events as a combination of pressure data (β_i) containing primaries (no direct wave) and the events of the vertical component of particle velocity (α_i). The scattering points connecting the two fields are located at the free surface. Note that we have used dotted lines to indicate the legs of scattering diagrams corresponding to the advanced waves which propagate backward in time. We will use this convention throughout the paper. (b) Our construction of virtual events in Fig. 5a has not included the free-surface-reflection events. Here we illustrate what happens when we include them in the vertical component of particle velocity. So the construction of virtual-reflection events here is a combination of pressure data (β_i) containing primaries, and the vertical component of particle velocity (α_i) containing free-surface-reflection events (ghosts and free-surface multiples). Again the scattering points connecting the two fields are located at the free surface. Note that this combination produces new configurations of virtual events, sometimes strange-looking virtual events.

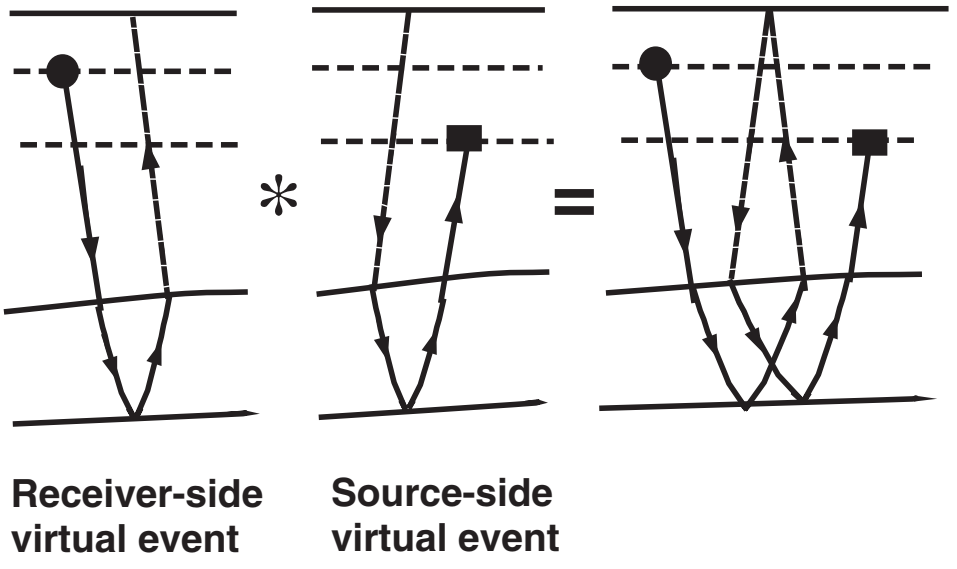

Fig. 6. An example of an event constructed as a combination of receiver-side and source-side virtual events. This is another strange-looking event. In terms of virtual acquisition, it simulates two simultaneous virtual experiments if the sources and receivers are at the same depth.

Let us remark that for the particular case of walkabove VSP (vertical seismic profile) experiments (see Ikelle and Amundsen, 2005), in which the receivers are positioned inside the subsurface through deviated wells, the field of virtual events is generally defined as follows:

$$P_V(\mathbf{x}_r,\omega;\mathbf{x}_s) = \int_{S_R} dS(\mathbf{x}) P^{-1}(\mathbf{x},\omega;\mathbf{x}_r) v_3(\mathbf{x},\omega;\mathbf{x}_s) \quad , \tag{5}$$

where S_R represents the surface in which receivers are located. Fig. 7 shows some of the virtual events that we can create by performing the scattering integral over S_R. We can notice that the virtual events in Figs. 7a and 7b are the same as those created in Figs. 5a and 5b with the scattering integral over S_0. These results provide a clear indication that virtual events can be refolded into data collected with sources and receivers in the subsurface. Notice also that if the upgoing events in, say, v_3, we can generate virtual events which are not present in the virtual towed-streamer field (see Fig. 7c), except when the surface S_R coincides with the actual location of one of the reflectors. We have not fully taken advantage of these last observations in our construct of virtual acquisitions. We hope to report progress on this front in the near future.

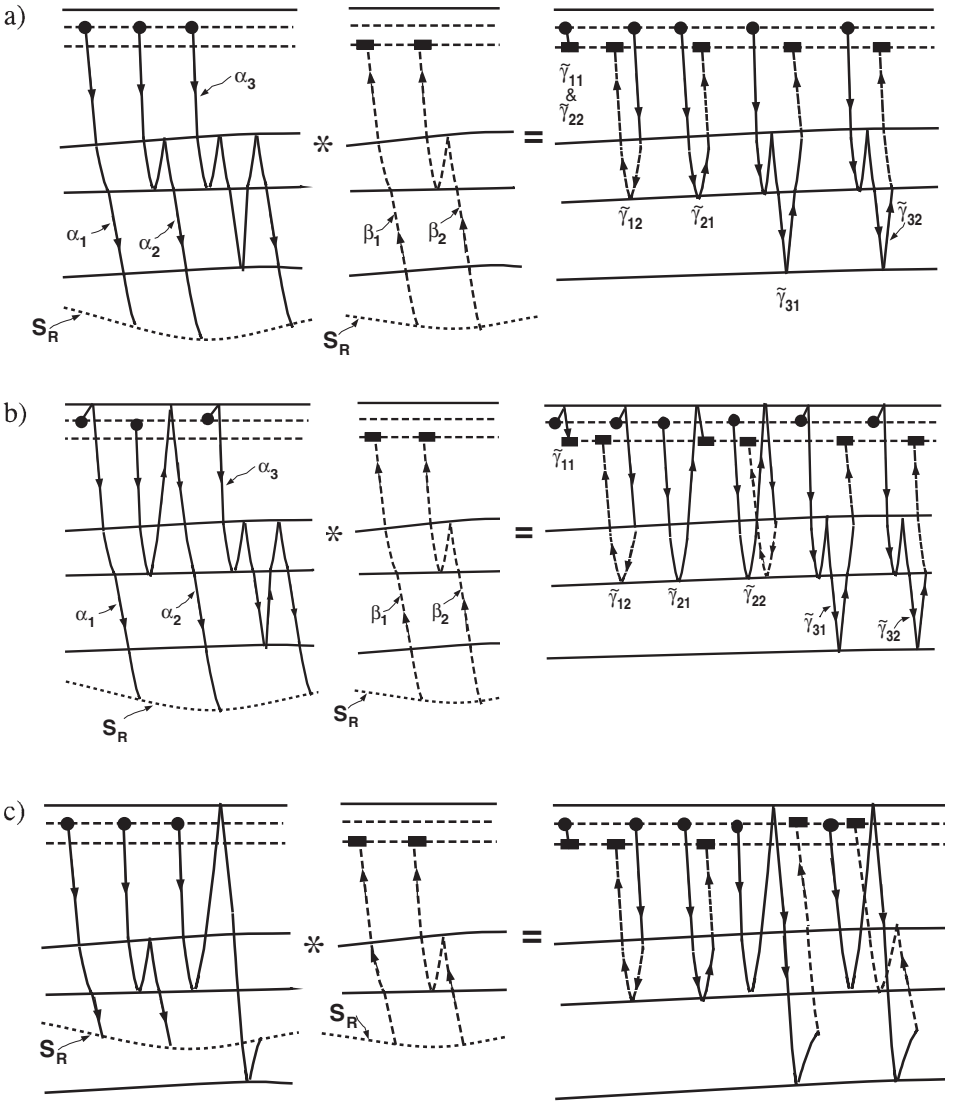

Fig. 7. (a) Examples of the construction of virtual-reflection events as a combination of pressure data and the vertical component of particle velocity. The scattering points connecting the two fields are now located on the surface S_R, inside the subsurface. This combination also produces the same virtual events as in Fig. 5a. (b) Examples of the construction of virtual-reflection events as a combination of pressure data, and the vertical component of the particle velocity containing free-surface-reflection events. The scattering points connecting the two fields are now located on surface S_R. This combination also produces the same strange-looking virtual events as in Fig. 5b. (c) In Figs. 6a and 6b, only downgoing waves are considered. Here we include upgoing waves in the vertical component of particle velocity. Notice new virtual events are created which are not present in Fig. 5. Moreover, some of the new virtual events (i.e., $\tilde{\gamma}_{31}$ and $\tilde{\gamma}_{32}$) includes bending at points which are not scattering points.

VIRTUAL SEISMIC ACQUISIION

Our objective in this section is to describe how one can construct data with sources and receivers inside the subsurface from standard data with sources and receivers near the sea surface for offshore or at the earth's surface for onshore. Let us now start by describing an alternative way of computing causal virtual events. Fig. 8a shows an example of a geological model with a number of real events associated with this model. Suppose now that we want to construct causal virtual events only with respect to interface Z1. We consider that the field P in (2) is made of event R1 only and v_3 contains the real events in Fig. 8a except R1. This separation is important for avoiding the generation of noncausal virtual events. Fig. 8b shows the virtual events one will obtain by using (2). Interestingly, we can construct all these virtual events by using the model in Fig. 8c. This model differs from the model in Fig. 8a in that the physical properties of layer 1 are made to be identical to those of layer 2. In addition, the sources and receivers in Fig. 8c are moved down to interface Z1 so that data resulting from this experiment describe only wave propagation through layers 2, 3, and 4. In other words, the virtual events with respect to interface Z1 are equivalent to moving the sources and receivers to interface Z1 and ignoring the medium above this interface. Hence the virtual events in Fig. 8b corresponding to data for a virtual acquisition with sources and receivers at the interface Z1. We can then remove internal multiples related to the interface Z1 and repeat the same process by starting with the data in Fig. 8c to generate data for a virtual acquisition with sources and receivers at interface Z2, and so on.

Notice that the aperture of virtual events is smaller than that of real events because virtual events have the same Fresnel zone as real events. As the virtual events are closer to the scattering point, it is normal that the aperture of virtual events be smaller than that of real events. This observation is consistent with the well-established fact that backward extrapolation of data, which is included in the construction of virtual events, reduces the data aperture. Notice also that when the interface in the subsurface at which the sources and receivers are located is not flat, the resulting data exhibits distorted moveout shapes, just as in land seismics when the air-solid interface is not flat. Let us add that if we use a combination of source-side virtual events and receiver-side virtual events, as in Fig. 6, we will end up simulating two simultaneous virtual experiments. We are currently evaluating the usefulness of the virtual acquisition associated with this combination.

The major practical challenge involved in constructing a virtual acquisition is segmentation of the data that ensure only causal virtual events are created at any given interface. We propose here an iterative technique of segmenting the data which is based on migration-velocity analysis with constant velocity.

a)

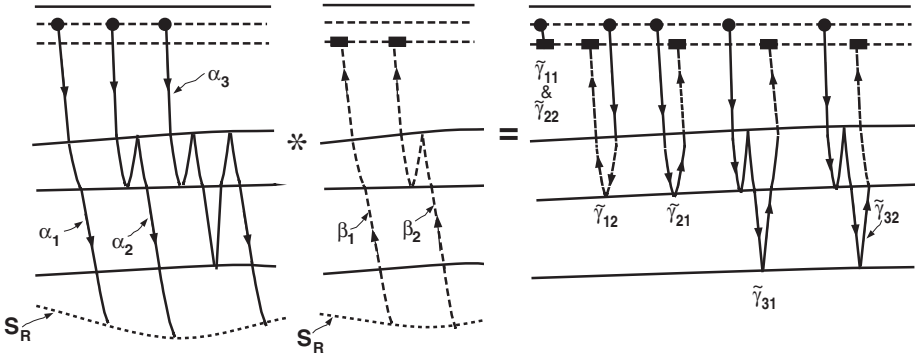
α3
α1
α2
SR
β1
β2
SR
γ̃11
&
γ̃22
γ̃12
γ̃21
γ̃32
γ̃31

b)

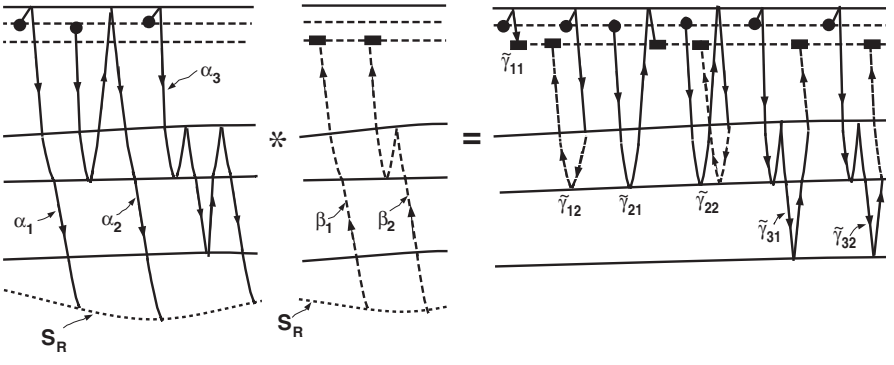
α3
α1
α2
SR
β1
β2
SR
γ̃11
γ̃12
γ̃21
γ̃22
γ̃31
γ̃32

c)

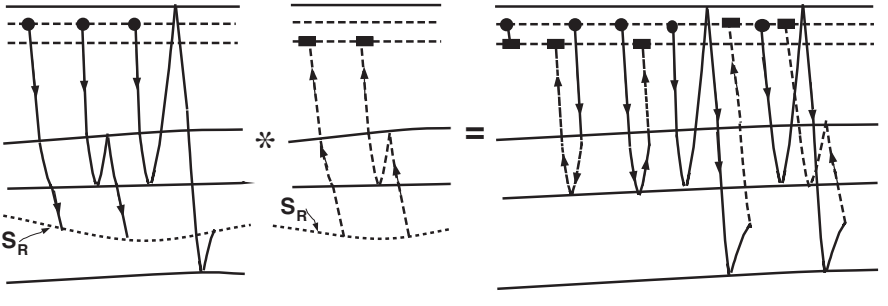
SR
SR

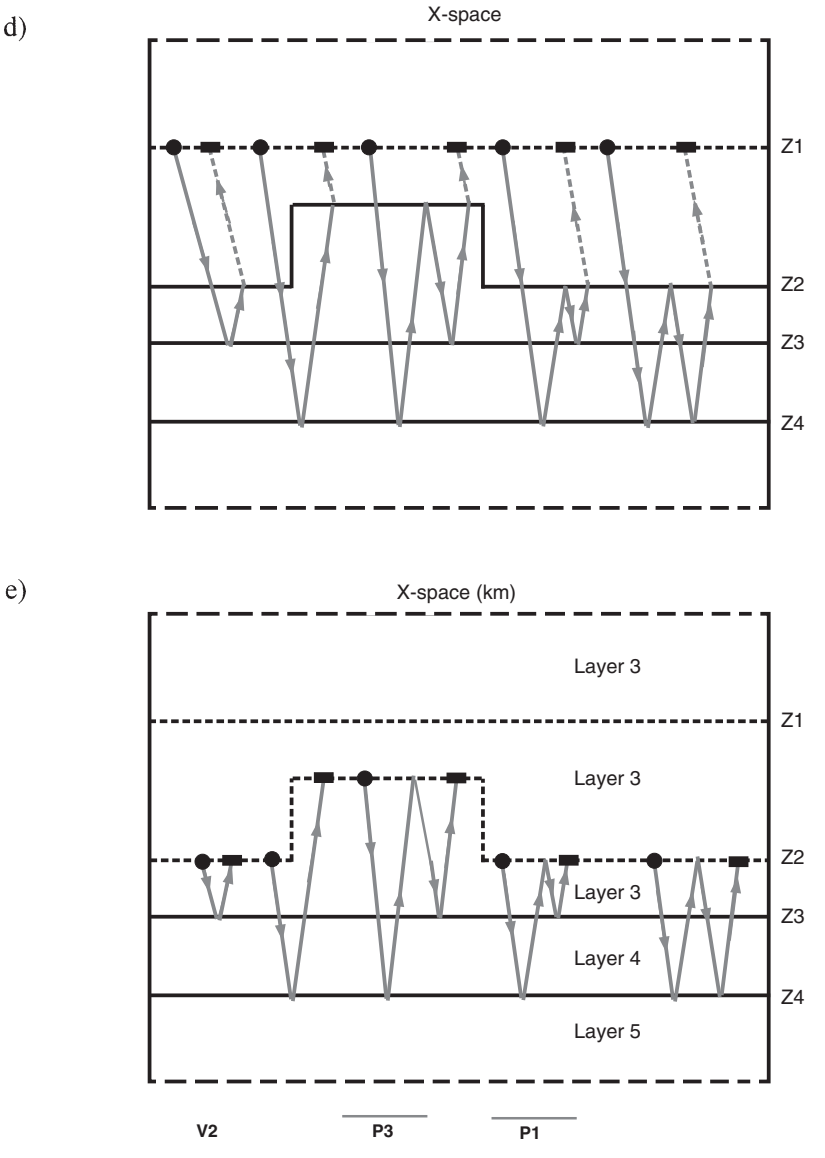

Fig. 8. (a) An example of a geological model with a number of real events associated with this model. Due to space only a limited number of events are shown. Notice that layers 1 and 5 are half-spaces. Z_i indicate the interface between the i-th layer and the $(i-1)$th layer. (b) Examples of causal virtual events associated with the interface at Z_1. (c) A virtual acquisition with sources and receivers at interface Z_1. Notice that the geological model here differs from the model in Fig. 8a in that the physical properties of layer 1 are made to be identical to those of layer 2. Notice also that the virtual events in Fig. 8b are equivalent to the real events here. (d) Examples of causal virtual events associated with interface Z_2. (e) A virtual acquisition with sources and receivers at interface Z_2. Notice that the geological model here differs from the model in Fig. 8a in that the physical properties of layer 1 and layer 2 are made to be identical to those of layer 3. Notice also that the virtual events in Fig. 8d are equivalent to the real events here.

The basic idea is to continuously move the boundary between $P(x_s,\omega,x)$ and $v_3(x,\omega,x_r)$ at each iteration. We will call this boundary the bottom-image generator (BIG) in analogy with the bottom-multiple generator (BMG) and bottom-internal-multiple generator (BIMG) introduced by Ikelle et al. (2005), Ikelle (2006), and Watts and Ikelle (2006) for the attenuation of free-surface and internal multiples. At the first iteration, we migrate the actual data with various constant velocities. We identify the constant velocity, which produces the optimal focus of the first reflector. We mute the rest of the image below this reflector, which we denote BIG1. We then demigrate the image above BIG1 to produce data that we then use to separate P and v_3 into data above and below BIG1. We denote $P^{(1a)}$ and $v_3^{(1a)}$ data above BIG1 and $P^{(1b)}$ and $v_3^{(1b)}$ data below BIG1. Then we produce the field of virtual events by crosscorrelating $P^{(1a)}$ and $v_3^{(1b)}$ using (2). We have generated data corresponding to ocean-bottom acquisition. We can then remove internal multiples related to the interface Z1 and repeat the same process using the virtual data obtained in the first iteration as input to produce data corresponding to sources and receivers at interface Z2, as described in Fig. 8, and so on. Table 1 summarizes the steps in this process.

Table 1. A summary of the key steps in identifying reflectors in the subsurface in which the virtual sources and receiver points will be located.

Step 1: Use the actual data to reconstruct the first reflector, which is the sea-floor reflection in the case of marine data. This step consists of applying a migration algorithm like the Stolt migration algorithm with a water velocity.
Step 2: We design the bottom-image generator (BIG) location using the migration result. The information above the BIG is assumed to be correct, and the remaining model below the BIG is a throwaway.
Step 3: We then use a demigration scheme of the image above the BIG obtained in Step 2 to also define the event-segmentation boundary for the data. The pressure data located above the segmentation boundary are considered as P^{-1} in (2) and the particle-velocity data below the segmentation boundary are used as v_3 in (2).
Step 4: Create virtual events using data above and below the segmentation boundary. We have created data corresponding to an acquisition with sources and receivers located at BIG under consideration. Remove internal multiples related to the BIG under consideration. One can also opt to perform a wavefield decomposition at this interface.
Step 5: Scan the field of virtual events with a velocity-migration; that is, we perform several constant-velocity migrations (e.g., Stolt, 1978) and select the migration result and the corresponding velocity that produce the best-focused image of the subsurface. We then define a BIG corresponding to the shallowest set of reflectors which are best-focused. We start again beginning with Step 2.

CONCLUSIONS

We have described one way of constructing data with sources and receivers inside the subsurface from standard data with sources and receivers near the sea surface for offshore, or at the earth's surface for onshore. We have used the concept of negative reflection events (also known as virtual events) to perform this construction. The issue of identifying the reflector in the subsurface at which the virtual source and receiver points must be located is also solved by using successive constant-velocity migration of virtual events.

ACKNOWLEDGMENTS

We would like to thank the sponsors of the CASP project for their comments and suggestions during the review process.

REFERENCES

Erez, I., 2006. The concept of virtual events and its applications to the attenuation of internal multiples and the separation of reflected and refracted waves: MSc Thesis, Texas A&M University, College Station, TX.

Ikelle, L.T., 2004. A construct of internal multiples from surface data only. Expanded Abstr., 74th Ann. Internat. SEG Mtg.,Denver: 2164-2167.

Ikelle, L.T., 2006. A construct of internal multiples from surface data only: the concept of virtual seismic events. Geophys. J. Internat., 164: 383-393.

Ikelle, L.T., Osen, A., Amundsen, L. and Shen, Y., 2004. Noniterative multiple-attenuation methods: linear inverse solutions to nonlinear inverse problems, II - BMG approximation. Geophys. J. Internat., 159: 923-930.

Ikelle, L.T. and Amundsen, L., 2005. An introduction to Petroleum Seismology: Investigations in Geophysics. SEG, Tulsa, OK.

Ikelle, L.T. and Gangi, A., 2005. New type of reflections in inhomogeneous media is revealed by an analysis of scattering diagrams of correlation-type representation theorem. J. Seismic Explor., 14: 1-12.

Ikelle, L.T. and Gangi, A., 2007. Negative bending in seismic reflection associated with time-advanced and time-retarded fields. Geophys. Prosp., 55: 57-69.

Jones, G.T., 2002. The uncertainty principle, virtual particles and real forces. Physics Educat., 37: 223-233.

Pendry, J.B., Holden, A.J., Robbins, D.J. and Stewart, W.J., 1999. Magnetism from conductors and enhanced nonlinear phenomena. IEEE Trans. Microwave Theory Tech., 47: 2075-2084.

Shelby, R., Smith, D.R. and Schultz, S., 2001. Experimental verification of a negative index of refraction. Science, 292: 77-79.

Smith, D.R., Pendry, J.B. and Wiltshire, M.C.K., 2002. Metamaterials and negative refractive index. Science, 305: 788-792.

Veselago, V.G., 1968. The electrodynamics of substances with simultaneously negative values of ϵ and η. Soviet Physics Uspekhi, 10: 509-514.

Watts, A.0. and Ikelle, L.T., 2006. Linear demultiple solutions based on the concept of bottom multiple generator (BMG) approximation: Some new results. Geophys. Prosp., 54: 492-497.

APPENDIX

COMPUTATION OF THE VERTICAL COMPONENT OF PARTICLE VELOCITY

In most towed-seismic acquisitions, we still record only the pressure field P. In these cases, we can compute the vertical component of the particle-velocity data from the pressure data, as follows (Ikelle and Amundsen, 2005):

$$v_3(x_s,y_s,\omega,x_r,y_r) = (1/Z)\int_{-\infty}^{+\infty}\int_{-\infty}^{+\infty} dk_x dk_y \sqrt{\{1 - c^2[k_x^2 + k_y^2]^2/\omega^2\}}$$
$$\times P(x_s,y_s,\omega,k_x,k_y)\exp\{i(k_x x_r + k_y y_r)\} \quad , \qquad \text{(A-1)}$$

where $P(x_s,y_s,\omega,k_x,k_y)$ is the Fourier transform of the actual pressure data $P(x_s,y_s,\omega,x,y)$ with respect to x and y, k_x and k_y are the wavenumbers associated with x and y, Z is the acoustic impedance of the water, and c is the velocity of the water. Strictly speaking, this formula is valid only when the receiver-ghost effects can be treated as part of the source signature (i.e., when the receiver depth is 5 m or less).